Silicon (2020) 12:3015–3026
https://doi.org/10.1007/s12633-020-00397-2

ORIGINAL PAPER

Effect of Silane-Coupling Modification on the Performance of chitosan-poly vinyl Alcohol-Hybrid Scaffolds in Bone Tissue Engineering

Farnaz Ghorbani[1] · Masoud Pourhaghgouy[2] · Tahere Mohammadi-hafshehjani[3] · Ali Zamanian[2]

Received: 27 April 2019 / Accepted: 28 January 2020 / Published online: 27 February 2020

Abstract
Biocompatibility and biodegradability characteristics of some polymers make them an excellent candidate to fabricate porous scaffolds for tissue engineering applications. However, the scaffold mechanical properties and biodegradation rate are vital for bone tissue replacement applications, which can be improved using proper fabrication techniques and cross-linker. In this investigation, Chitosan-polyvinyl alcohol scaffolds were prepared by freeze-drying technique utilizing various weight ratios of 3-Glycidoxypropyl trimethoxysilane (GPTMS) as a bioactive inorganic crosslinker. SEM micrographs indicated interconnected porous structures of cross-linked scaffolds while the average diameter of pores increased as a function of cross-linker enhancement. FTIR analysis was performed to confirm interactions among organic and inorganic components. The mechanical strength test represented that increasing GPTMS content improves the compressive strength of samples. The absorption capacity of the scaffolds in the PBS solution exhibited a decrease in water uptake and biodegradation by increasing silane coupling agent concentration. The formation of needle-like apatite particles proved suitable bioactivity of cross-linked samples. Moreover, MTT assay and ALP expression showed an acceptable adhesion, spreading, proliferation, and differentiation of MG-63 cells on the silane-contained scaffolds. Obtained results warrant further preclinical and clinical evaluations.

Keywords Tissue engineering · Scaffolds · Cytocompatibility · GPTMS · Chitosan · PVA

1 Introduction

In tissue engineering, scaffolds have been applied to obtain a temporary artificial extracellular matrix (ECM) with the purpose of supporting cell attachment and guiding three-dimensional (3D) tissue formation. Developing new scaffolds by polymer blends has drawn a lot of attention in recent decades [1, 2]. Polymeric blends create better properties to regenerate the desired tissue structures in comparison with single ones [3, 4]. A wide variety of polymeric blends have been investigated for the engineering of soft tissues such as Poly(lactic-co-glycolic-acid) (PLGA) and gelatin [5], corn starch and polystyrene [6], poly(lactic acid) and poly(vinyl acetate) [7], poly (vinylidene fluoride) and ultrahigh-molecular-weight polyethylene [8], etc. Among these polymers, chitosan is playing an ideal role in tissue engineering scaffolds and attracting a keen interest in soft tissue engineering [2]. Chitosan is a linear polysaccharide of β-[1- 4]-linked 2-acetamido- 2-deoxy-D-glucopyranose and 2-amino-2-deoxy-D-glucopyranose and considered as second abundant biopolymer [3]. Due to its biocompatibility, biodegradability, non-toxicity, and antimicrobial properties, it has been used in many applications [9]. However, the weak mechanical strength of the chitosan-based scaffolds limits its clinical applications [10]. Thus, several investigators have attempted to develop new chitosan scaffolds with desirable properties that can replace the natural ECM. Recent evidence suggests that blends of synthetic and natural polymers show a new type

✉ Farnaz Ghorbani
farnaz_ghorbani.1991@yahoo.com

✉ Ali Zamanian
a-zamanian@merc.ac.ir

[1] Department of Orthopedics, Shanghai Pudong Hospital, Fudan University Pudong Medical Center, Shanghai, China

[2] Biomaterials Research Group, Department of Nanotechnology and Advanced Materials, Materials and Energy Research Center, Tehran, Iran

[3] Functional Interface Department, Karlsruhe Institute of Technology, Eggenstein-Leopoldshafen, Germany

of materials and have attracted much attention [3]. Therefore, blending chitosan with other polymers would be an effective way of producing new scaffolds. Poly (vinyl alcohol) (PVA) is one of the most common synthetic polymers and because of its biocompatibility, non-toxic, and chemical properties have been attained great interest for biomedical applications. Hydrophilicity of the PVA plays a significant role in the extension of its bio-applications owing to considerable improvement in biological behavior [11]. A published study showed that chitosan and PVA have many hydroxyl groups in their chemical structure that lead to formation of hydrogen bonds between the hydroxyl groups of chitosan and PVA and promote the localized stability and improvement of the miscibility [12].

In most medical applications, the chain of hydrophilic polymeric scaffolds should be cross-linked in order to have better mechanical and biodegradation properties. Different kinds of cytotoxic reagents have been used as cross-linking agents such as epoxy compounds, formaldehyde, and glutaraldehyde, which may damage the biocompatibility of the scaffolds [13]. In fact, the possible presence of some unreacted cross-linking agents inside the scaffold may lead to the formation of toxic products during in-vivo biodegradation [14]. For this reason, growing interest has been recently attained to utilize low toxic cross-linking agents. Furthermore, induction of osteoconductivity through the scaffold can be profitable in bone regeneration [15]. Thus, many different bioactive materials have been added to the scaffolds to improve the bioactive properties of constructs [16–18] . So, a combination of polymers and bioceramics to fabricate hybrid scaffolds for bone tissue engineering applications attracts many scientists. In fact, bioceramics, including HA and other bioactive silicate glasses, exhibit osteoconductivity and provide the ability of bonding with connective tissues that can improve the bioactivity of polymeric scaffolds [19, 20]. However, high values of these bioactive particles as a dispersed phase in polymeric solutions can enhance problems associated with weak interfacial bonding and particle agglomeration, which may cause more fracture, cytotoxicity problems related to ion release from glasses and the lack of biodegradation of HA in the body [21, 22].

The silane coupling agent named 3- glycidoxypropyltrimethoxysilane (GPTMS) includes epoxy and methoxysilane groups, which is mostly used for modification of hydrophilic materials [23]. A previous study clearly indicated that there is a direct relationship between the amount of GPTMS density as a cross-linker and the scaffolds biodegradation rate [14]. The cross-linked composite scaffolds also showed bioactivity due to the existence of silanol groups derived from GPTMS. Besides, the released ions such as Si ions were not cytotoxic after degradation of the scaffold [24].

In this study, the influence of GPTMS on the physicochemical, mechanical, and cytocompatibility of PVA-chitosan scaffolds has been determined. In this regard, structures with various compositions were fabricated through the freeze-drying process. The results may help the researchers in a similar field of study to optimize the density of GPTMS in cross-linked networks and hope to design a suitable tissue-regenerative composite material.

2 Experimental

2.1 Materials

PVA (98% hydrolyzed, the average molecular weight of 72,000 g/mol), acetic acid (AA, M_w 60.05 g/mol), ethanol (M_w = 46.07 g/mol), and 3-glycidoxypropyltrimethoxysilane (GPTMS, M_w 236.34 g/mol) were purchased from Merck (Germany). Chitosan (medium molecular weight), sodium hydroxide (NaOH, M_w 40.00 g/mol), thiazolyl blue tetrazolium bromide (MTT, M_w = 414.32 g/mol), dimethyl sulfoxide (DMSO, 1X), L-glutamine (M_w = 146.14 g/mol), non-essential amino acid solution (100X), and ethidium bromide (M_w = 394.31 g/mol) were supplied from Sigma-Aldrich (USA). Phosphate buffered saline powder (PBS, pH 7.2–7.4) and simulated body fluid solution (SBF, pH 7.4) were purchased from Aprin Advanced Technologies Development Co. Ltd. (USA). Dulbecco's modified eagle's medium (DMEM) was purchased from Mehregan Biotechnology Co. Ltd. (Iran). Fetal bovine serum (FBS) and penicillin-streptomycin were purchased from Gibco-BRL, Life Technologies Co. Ltd. (NY). Alkaline phosphatase kit (ALP) was purchased from MAN Co. Ltd. (Iran). All chemicals were used directly without further purification. Aqueous solutions were prepared with doubly distilled water.

2.2 Preparation of Scaffolds

An equal amount of chitosan and PVA (50:50 weight ratio) were dissolved in 2% (*v*/v) acetic acid to obtain a concentration of 3% (*w*/*v*). Then GPTMS in a different weight ratio of 0.5:1, 1:1, and 1.5:1 (GPTMS:polymer) was added to the solutions and stirred for 2 h at room temperature. The prepared solutions were poured into cylindrical molds with 10 mm diameter and frozen at −20 °C. Then all the frozen samples were transferred into freeze-dryer (FD-10, Pishtaz Engineering Co. Iran) and lyophilized at the temperature of −58 °C and pressure of 0.5 Torr for 48 h to ensure that all the ice crystals have been entirely sublimated. All the scaffolds were neutralized by soaking in 0.1 M sodium hydroxide (NaOH) for 1 h, washing with deionized water (3 times), and soaking again in deionized water for half an hour. Table 1 shows a list of the prepared solutions and their codes.

Table 1 The components, notation, and ratio of different freeze-drying scaffolds studied in this work

Codes	Composition (Weight ratio)	Freezing temperature (C)	Polymer: GPTMS (weight ratio)
CP0.5G	Chitosan:PVA 50:50	−20	1:0.5
CP1G	Chitosan:PVA 50:50	-20	1:1
CP1.5G	Chitosan:PVA 50:50	-20	1:1.5

2.3 Scaffolds Characterization

2.3.1 Morphology Determination

The morphology and microstructure of the synthesized structures (CP0.5G, CP1G, and CP1.5G) scaffolds were evaluated using Scanning Electron Microscopy (SEM, Stereoscan S 360-Leica, UK) at the acceleration voltage of 15 kV. The polymeric samples were coated with a layer of gold by sputtering (Emitech K450X, Ashford, UK).

Image measurement software (KLONK Image Measurement Light, Edition 11.2.0.0) was used to characterize the SEM micrographs in the original magnification of 50X. At least five different SEM micrographs and 25 measurements at each image were performed to determine the average and standard deviation of the results.

The porosity of scaffolds was calculated by using the Eq. (1) [5]. Where $\rho_{scaffold}$ is the density of the freeze-dried scaffold, ρ_{solid} is the density of the bulk polymer. The apparent density of the scaffolds was accurately measured by using a density bottle method.

$$\text{Porosity}\% = 1-(\rho_{Scaffold}/\rho_{Solid})*100 \quad (1)$$

2.3.2 Fourier Transform Infrared Spectrum (FTIR)

Chemical characterization of scaffolds was examined by Fourier transform infrared analysis with a Nicolet Is10 FTIR spectrophotometer (USA). 1 mg of scraped samples mixed with 300 mg of KBr and pelletized under vacuum. Then, pellets were analyzed between 400 and 4000 cm^{-1} with a resolution of 4.0 cm − 1 and 8 scans.

2.3.3 Mechanical Testing

Mechanical properties of the scaffolds were determined by a compression strength test system (Santam, STM −50, Iran) with a crosshead speed of 0.5 mm/min and a load cell of 100 N. All the samples were cut to 12 mm height. At least five samples were analyzed for each type of scaffold to calculate the average and standard deviation of the results.

2.3.4 Swelling Test

The swelling of the prepared cross-linked scaffolds was tested with immersing the samples in falcon tubes containing 50 ml of PBS solution incubating in-vitro at 37 ± 0.5 °C and the rotational speed of 30 rpm for different period times (1, 3, 6, 9, and 24 h). After immersion of the scaffolds in PBS solution at various times, the amount of PBS uptake was determined after removing the samples from the medium and wiping off the excess surface PBS with filter papers. The percent of swelling is given by using the Eq. (2) [25]:

$$\text{Swelling ratio}\% = [(W-W0)/W0]*100 \quad (2)$$

Where W_0 is the original weight, and W is the wet weight of the sample. Each swelling examination was repeated five times to determine the average and standard deviation.

2.3.5 Biodegradation Test

Biodegradation study of the scaffolds was performed with incubating the samples in 50 ml PBS (pH 7.4) at 37 ± 0.5 °C and the rotational speed of 30 rpm for different period times (1, 2, 3, and 4 weeks). After each biodegradation period, the samples were washed with distilled water and freeze-dried (temperature of −58 °C and pressure of 0.5 Torr for 24 h). In order to find out the biodegradation rate, the samples were weighed, and the biodegradation index was calculated based on the mass loss using the Eq. (3) [26]:

$$\text{Biodegradation ratio}\% = [(W-W0)/W0]*100 \quad (3)$$

Where W_0 is the wet weight, and W is the dry weight of the samples after soaking in PBS. Each biodegradation experiment was repeated five times to determine the average and standard deviation.

2.3.6 In-Vitro Bioactivity Assay

In-vitro bioactivity of the composite scaffold (CP1G) was evaluated by soaking samples in 50 ml SBF solution under shaking at 37 ± 0.5 °C with the rotation speed of 30 rpm (Thermoshaker, LS-100, Thermo Scientific, USA) for 3, 7, and 14 days. The bioactivity analysis was performed as described by Kokubo et al. [27]. So, the SBF solution was refreshed every 2 days. After each immersion time, samples were washed with deionized water and freeze-dried (temperature of −58 °C and pressure of 0.5 Torr for 24 h) to keep their structure. Phase analysis of the composite scaffolds was conducted using XRD (XRD, Philips

PW3710) analysis with monochromatic Cu-Kα radiation under the operating conditions of 40 kV and 30 mA. A comparison of XRD patterns with JCPDS standards was carried out to identify the crystalline phases. The morphological and microstructural study of the apatite formation on scaffolds after immersing in SBF was characterized by SEM-EDX (SEM, Vega3, TESCAN, Czechoslovakia) at an accelerating voltage of 15 kV. All samples were coated with a thin layer of gold in double 30-s consecutive cycle at 45 mA to reduce charging and produce conductive dried surface. Chemical characterization of apatite-like layers on the scaffolds was examined by Fourier transform infrared analysis with a Nicolet Is10 FTIR spectrophotometer (USA) between 400 and 4000 cm^{-1} with a resolution of 4.0 cm^{-1} and 8 scans.

2.4 In-Vitro Study in Contact with MG-63 Osteosarcoma Cells

The in-vitro cytotoxicity of the CP1G scaffolds was tested using the MG-63 osteosarcoma cells. The cells were kept in Dulbecco's Modified Eagle Medium (DMEM) supplemented with 10% fetal bovine serum (FBS) and streptomycin/penicillin 100 U/mL and 1.2% glutamine. The culture was kept at 37 C in a wet atmosphere containing 5% CO_2. When the cells reached 80% confluence, they were trypsinized with 0.25% trypsin containing 1 mM EDTA. In the 24-well plate, $5*10^5$ cells/ml were seeded in each well. The scaffold specimens were sterilized under UV light for 2 h and then kept in 75% alcohol solution overnight. After that, the samples were washed three times with PBS and twice with cell culture medium. The sterilized scaffolds were washed three times with sterile phosphate-buffered saline (PBS) and transferred to individual 24-well tissue culture plates. After 48 h of incubation, the samples were rinsed with PBS twice, and then the cells were fixed with 3% glutaraldehyde solution in PBS. After 30 min, the specimens were rinsed again with PBS and kept in PBS at 40 °C. Then, the specimens were fixed with 1% Osmium tetroxide (Polyscience, Warmington, PA, USA) followed by dehydration through ethanol solutions of ascending concentrations (30, 50, 70, 90, and 100%) for about 20 min at each concentration. The specimens were then dried in air. After being dried completely, the specimens were mounted on copper stubs, coated with gold, and observed by SEM (Philips XL30, Netherland) at an acceleration voltage of 15 kV.

The cell viability assay of specimens was investigated by MTT test, as described in our previously published work [28]. For the MTT test, the cells were exposed to the samples for 3 and 5 days, as described above. After each predetermined incubation time, the DMEM was removed and replaced with a fresh medium containing 10% MTT solution (3-(4, 5-Dimethyl-2- thiazolyl) 2, 5-diphenyl-2Htetrazolium bromide) and left for 2 h at 37 °C. The cells were then treated with dimethyl sulfoxide DMSO for 30 min. The optical density (OD) of the samples, as a cell viability indicator, was measured by ELISA (enzyme-linked immunosorbent assay) reader at a wavelength of 570 nm with a reference filter of 620 nm. The cells cultured in medium without scaffolds were served as a control (100% cell viability).

Alkaline phosphatase activity was evaluated according to the method described by Lowry et al. [29]. To determine alkaline phosphatase (ALP) activity, 5×10^5 MG-63 cells were seeded on scaffolds as described above. Lysing the cells followed by 0.1% Triton X-100 to the scaffolds and freeze-thawing at 37 °C to evaluate ALP activity at days 3 and 5 was performed according to the MAN company instructions. The lysis cells were incubated with p-nitrophenyl phosphate (PNPP) solution at 37 °C for 30 min, and the reaction was stopped with NaOH (1 N). ALP activity was determined at 405 nm.

2.5 Statistical Analysis

All experiments were performed in five replicates. The results were given as mean ± standard error (SE). Statistical analysis was conducted by one-way ANOVA and Tukey test with significance reported when $P < 0.05$.

3 Result and Discussion

3.1 Morphology and Porosity of Scaffolds

SEM images (Fig. 1) depict high porosity and interconnected pores for all chitosan-PVA-GPTMS (CPG) scaffolds and illustrate homogeneous integrity of constructs. Furthermore, it is shown that the concentration of GPTMS in the initial solution affect the final structure of scaffolds. The porosity of each scaffold was also precisely obtained and they were around 91.23%, 89.87%, and 88.52% for CP0.5G, CP1G, and CP1.5G scaffolds, respectively (Table 2).

Freeze-drying procedure lead to formation of cellular morphology and interconnected pore networks due to the random ice crystals growth [30]. However, the final properties of the microstructure were affected by their compositions. Here, we propose a cross-linked scaffold in which addition of GPTMS resulted in a suitable microstructure of the prepared scaffolds for bone tissue engineering. According to Fig. 2, with an increase in GPTMS amount, larger pore size and more homogenous structure were created in the scaffolds, which facilitates pore formation without plastic deformation. Moreover, a better distribution of pores was obtained by the increase in GPTMS content. Finally, the critical role of scaffold's porosity and pore morphology to allow migration and proliferation of cells and to support the exchange of nutrients and waste products with the microenvironment should be considered [31].

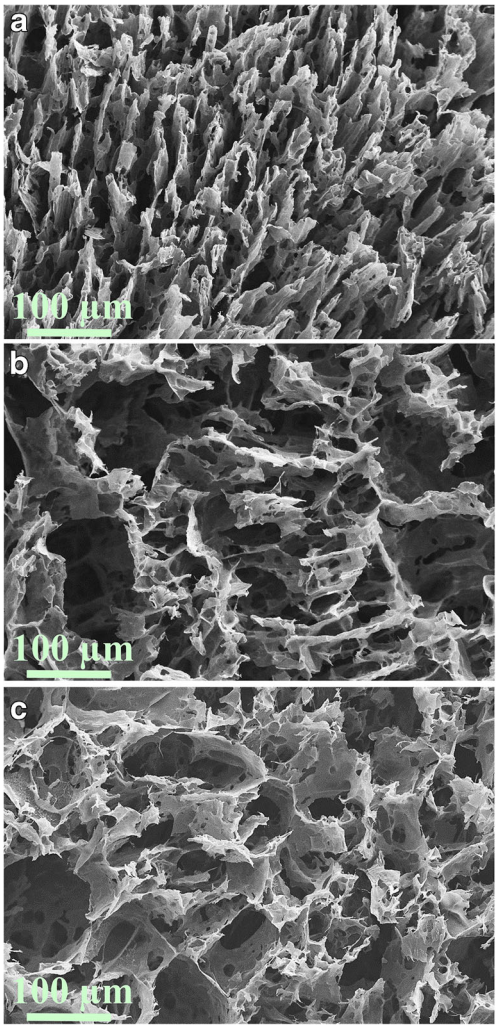

Fig. 1 Typical SEM micrographs of the surface microstructure of the freeze-drying CPG porous scaffolds with different GPTMS contents. **a** CP0.5G, **b** CP1G, **c** CP1.5G. Magnification of a, c and e is 200X

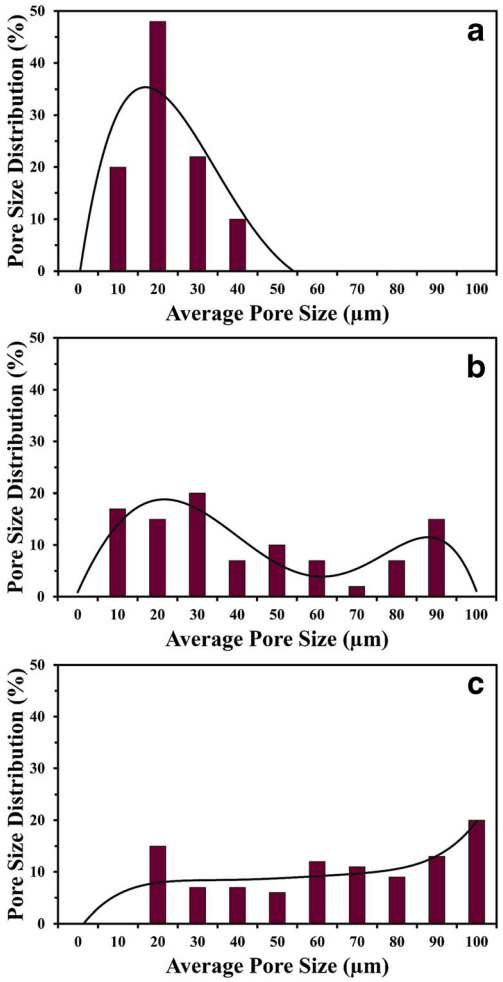

Fig. 2 The pore size distribution of different cross-linked scaffolds **a** CP0.5G, **b** CP1G, **c** CP1.5G. The pore size increased as a function of GPTMS enhancement

3.2 Chemical Bonding

Figure 3 shows the FTIR spectra of PVA, chitosan, GPTMS, and CPG blends. For the chitosan sample, the absorption peaks around 846 and 1150 cm^{-1} are assigned to the saccharide structure [32]. Also, the peaks at 1740, 1480, and 1346 cm^{-1} are related to the vibration of amide I, II, and III peaks, respectively [16, 33], and the peak is shown at around 2899 cm^{-1} is because of the C-H stretch vibrations. Moreover, the broad peak observed at 3447 cm^{-1} is due to amine N-H symmetrical vibration and hydroxyl groups. The infrared spectrum of PVA around 3440 cm^{-1} and 2921 cm^{-1} have been reported as –OH and CH_2 stretching vibrations, respectively [34, 35]. Also, the primarily observed absorption bands of PVA are the result of the 1734 cm^{-1} stretch of C=O group and 1098 cm^{-1} of C-O and 850 cm^{-1} of C-C from acetate

Table 2 Porosity, mechanical strength, absorption, and biodegradation rate of the prepared scaffolds

Sample codes	Porosity (%)	Compressive strength (MPa)	24-h PBS absorption rate (%)	4-Weeks biodegradation rate (%)
CP0.5G	91.23	0.38 ± 0.03	1633.12 ± 33.23	35.19 ± 6.36
CP1G	89.87	0.65 ± 0.02	1361.89 ± 34.64	33.72 ± 3.53
CP1.5G	88.52	0.71 ± 0.007	1140.52 ± 49.49	29.14 ± 0.70

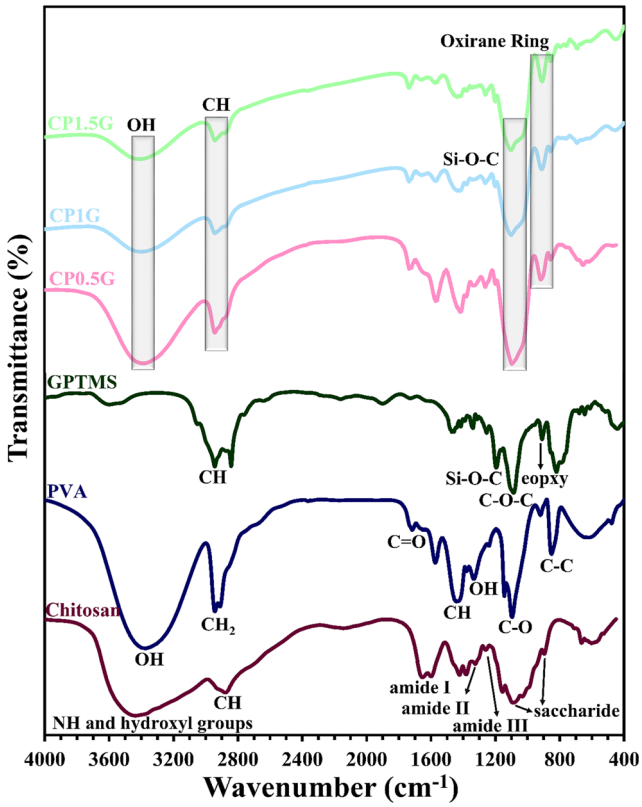

Fig. 3 FTIR spectra of chitosan, PVA, GPTMS, and different scaffolds: CP0.5G, CP1G, and CP1.5G

groups. Furthermore, the absorption peak at 1000–1100 cm^{-1} is caused by the stretching vibration of C-O groups in PVA. Furthermore, in the FTIR spectrum of GPTMS, the vibration at 2962.02 cm^{-1} and 1094.24 cm^{-1} are related to C-H and C-O-C stretching, respectively [34]. The bonds at 1024 cm^{-1} indicate Si-O stretching vibration. Another peak around 1261 cm^{-1} is the result of Si-C stretching vibration, and oxirane ring vibration occurs at 905 cm^{-1}. Also, the FTIR spectrum of CPG scaffolds illustrates the O-H stretching vibration at 3434.48 cm^{-1} and C-H stretching vibration at 2924.18 cm^{-1}, respectively. The disappearance of the absorption band at 910 cm^{-1} (oxirane ring) and an increase in the absorbance of the peak at 1000–1100 cm^{-1} indicate cross-linking reactions. Broadening is due to the adsorption of the Si-O-C bonds, which may be created following the condensation reactions between Si-OH groups from hydrolyzed GPTMS and C–OH groups from PVA or the amino group of chitosan [36, 37]. In addition, the absorption band at 920 cm^{-1} is caused by the Si-OH stretching [14].

According to the previous studies [34, 38] and the FTIR results, it can be concluded that in this study, GPTMS successfully acted as a cross-linker and reacted with amine groups of chitosan and the hydroxyl groups of PVA. For this purpose, the ring-opening reaction of epoxy groups of GPTMS and deprotonation of hydroxyl groups of PVA and chitosan have occurred. This epoxy ring of GPTMS can be reacted with the hydroxyl groups of PVA or the hydroxyl or amine groups of chitosan and create ether bonds. On the other hand, Trimethoxy groups of GPTMS hydrate and acid-catalyzed reactions create pendant silanol groups. The condensation reaction leads to the formation of Si-O-Si.

3.3 Compression Test

The compression test was performed to evaluate the effects of the GPTMS cross-linking degree on the mechanical properties of the CPG scaffold. The compression test results are presented in Table 2. It was well known that the porosity and composition of scaffolds are the most significant contributions to the mechanical properties. Based on the results, the compression behavior was influenced by the compositions. Increasing the inorganic phase (GPTMS) led to better compressive strength. According to a previous study [39], the added values of GPTMS to the solution lead to higher compressive strength, and consequently, higher mechanical stress is needed to deform the structure. The compressive strength increased with the enhancement of the GPTMS content (0.38 MPa to 0.65 MPa from CP0.5G to CP1G). Increasing the ratio of polymer:GPTMS to 1:1.5, improved the scaffold strength to approximately 0.71 MPa (Fig. 4). The compressive strength of CP1.5G was almost two times higher than that of CP0.5G which shows the effect of cross-linking content on the strength of scaffolds. The prepared constructs contain bridging skeletons like (Chitosan/PVA)-(GPTMS skeleton)-Si-O-Si-(GPTMS skeleton)-(Chitosan/PVA). Therefore, the increase in strength of samples could be related to the fact that the larger content of GPTMS introduces many of Chitosan/PVA-Chitosan/PVA-bridging bonds, which create tight

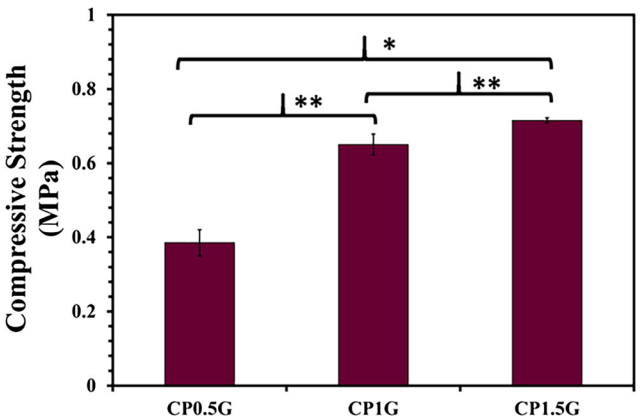

Fig. 4 Compressive strength of CP0.5G, CP1G, and CP1.5G scaffolds. (*$P = 0.0002$, **$P = 0.00005$; ANOVA, all pairs were compared using Tukey's test)

intermolecular bonds [40]. Therefore, the CP1.5G scaffold has a more rigid matrix and higher strength than the CP0.5G scaffold does.

3.4 Swelling and Biodegradation Behavior

The maintenance of the scaffold shape and cell growth are affected by the amount of water absorption. However, the moisture content is one of the main factors showing the biocompatibility of scaffolds, physiological stability, and permeability to biomolecules [33]. The higher water absorption means having a larger area/volume ratio, which might be suitable for cell infiltration as well as a cell attachment [41, 42]. In this work, the effect of GPTMS content on the water absorption of CPG scaffolds was examined. The obtained data were recorded after the 1, 3, 6, 9, and 24 h of the test (Fig. 5(a)). Hydroxyl groups of PVA and both hydroxyl and amine functional groups of chitosan provide proper sites for the formation of hydrogen bonding between the substrate and water, which can improve the scaffold hydrophilicity and water absorption capacity [43, 44]. The lower swelling rate for CP1.5G is due to the presence of more hydrophobic siloxane chains of GPTMS instead of hydrophilic hydroxyl and amine groups and the lower porosity. An increase in GPTMS content resulted in a decrease in water uptake of samples after only 1 h incubation in the PBS solution. It can be observed that the changes in water absorption are related to the GPTMS content and it decreased from 1633.12% for CP0.5G to 1361.89% for CP1G and 1140.52% for CP1.5G after 1 h. The higher amount of GPTMS leads to more Chitosan-PVA- Chitosan-PVA /bridging bonds. Thus, it was found that CP1.5G has a more rigid matrix than CP0.5G and a lower degree of water uptake [40]. Furthermore, a higher amount of GPTMS led to lower porosity. So, the water-absorbing capacity reduction can be attributed to the porosity reduction of the structure. Higher structure porosity enhances the water penetration in the structure and leads to more swelling ratio [45]. However, by increasing the immersion time from 1 h to 24 h, the water uptake slightly changed.

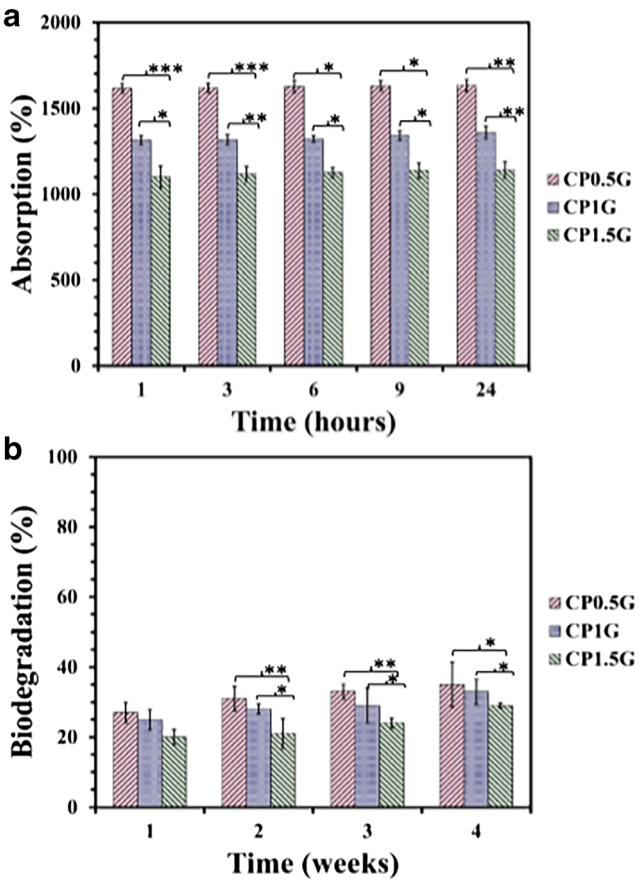

Fig. 5 **a** Uptake capacity and **b** biodegradation rate of the composite scaffolds in different time intervals. Increasing GPTMS content reduced absorption capacity and degradation rate. (*$P < 0.05$, **$P = 0.003$, ***$P = 0.006$, ANOVA, all pairs were compared using Tukey's test)

The aim of biodegradation tests on CPG samples was an investigation of their stability in the PBS solution. It can be seen that CP0.5G, CP1G, and CP1.5G weight loss were 35.19%, 33.72%, and 29.14%, respectively, after 1 week (Fig. 5(b)). According to the results, the reduction of water uptake, an increase in mechanical strength, and greater cross-linking extent in scaffolds were due to higher values of GPTMS, which influenced the biodegradation rate. Biodegradation ratio was slightly lower for CP1.5G compared with CP1G and CP0.5G scaffolds. Also, an increase in GPTMS content reduced the scaffold porosity amounts. It means that higher GPTMS content ends to lower porosity and absorption capacity and finally prevent rapid biodegradation. The same results were observed in Tonda-turo et al. [14] investigation. In fact, differences in the biodegradation rate of scaffolds can also be attributed to their matrix structure.

3.5 Bioactivity Behavior of SBF Solution

The final results of the analysis mentioned above demonstrated that there is a balance between mechanical, swelling, and biodegradation behavior of CP1G scaffolds. Therefore, this study was followed on the scaffolds with the best features compared to the other ones. The surface of the CP1G scaffolds illustrated morphological changes after immersion in the SBF solution. Many fine, needle-like particles were formed on the surface of the samples within 14 days, which are observed SEM observation (Fig. 6). According to the results, the number of precipitated particles increased, and apatite-like layers become denser as a function of time. So, after 14 days, the surface of the scaffold was almost entirely covered with needle-like particles.

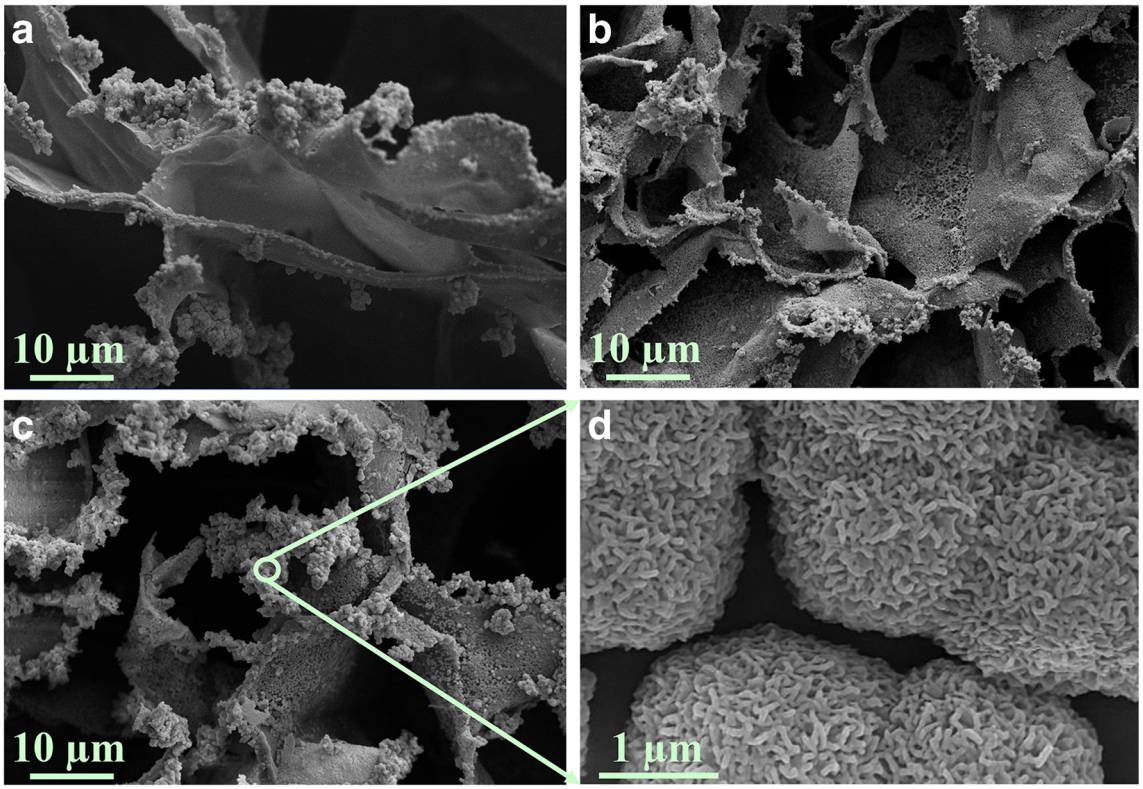

Fig. 6 SEM micrographs of CP1G scaffolds after soaking in SBF solution for **a** 3, **b** 7, and **c** 14 days. Silane-contained scaffolds can support the mineralization of hydroxyapatite-like layers

EDX results (Fig. 7) confirmed that Ca and P covered the surface of structures after 3 days and continued to increase with the immersion time (7 and 14 days). The presence of GPTMS in scaffolds plays the main role in apatite formation. GPTMS is known as one of the silane-coupling agents, which contain an epoxy group and methoxysilane groups. The epoxy group interacts with the hydroxyl group of PVA as well as with amino groups of chitosan chains [46]. Also, after hydrolysis of methoxysilane groups, silanol groups create. The formation of these Si-OH groups attracts Ca^{2+} ions from the SBF to form an amorphous calcium silicate on the scaffolds [47]. So, after the soaking period, the combination of calcium silicate with SBF ions leads to the formation of amorphous calcium phosphate particles. FTIR results are shown in Fig. 8(a). The band at 1090 cm^{-1} is attributed to Si-O-Si vibrations. The broad-band at 3440 cm^{-1} and the small peak at 1630 cm^{-1} are the results of O-H stretching. The peak at 607 cm^{-1} is due to phosphate absorption bands. Also, the band at 850 cm^{-1} caused by C-O vibration [48, 49]. These peaks are a function of apatite formation on the surface of the silane-contained scaffolds, in which the observed peaks become sharper with increasing immersion time. The XRD analysis is shown in Fig. 8(b) described that after immersion of the scaffold in SBF for 3 days, small peaks were detected in 2θ angel of 26, 31.8, 39.8, 46.7, and 53.3 °. This event corresponded to the dominant (210),(211), (130), (222) and (004) reflection planes in a referenced HA (JCPDS 72–1243) [50, 51]. The intensity of these peaks increased with immersion time.

3.6 In-Vitro Biocompatibility

In order to investigate the cell adhesion and proliferation capability of the proper sample, MG-63 osteosarcoma cells were cultured on the surface of CP1G samples, and the morphology of the cultured cells was observed by SEM. SEM image in Fig. 9(a) showed the morphology of cultured-MG-63 cells on the CP1G scaffolds after 48 h. Accordingly, cells were attached well on the surface of CP1G, and filopodia formation has occurred after 48 h. The high swelling capacity and porosity of the fabricated scaffold provide a suitable environment for cell adhesion and proliferation.

The absorbance obtained from an MTT assay of the MG-63 cells is shown in Fig. 9(b). After 3 days, the absorbance intensity of CP1G scaffold was 0.09, which increased to 0.22 after 5 days. The MTT assay results indicate the absorbance intensity of the CP1G scaffold was higher than the control sample after 5 days. Therefore, it was suggested that the samples were nontoxic to MG-63 cells and may be as good samples to be used as tissue scaffolds. Although Si ion release improves

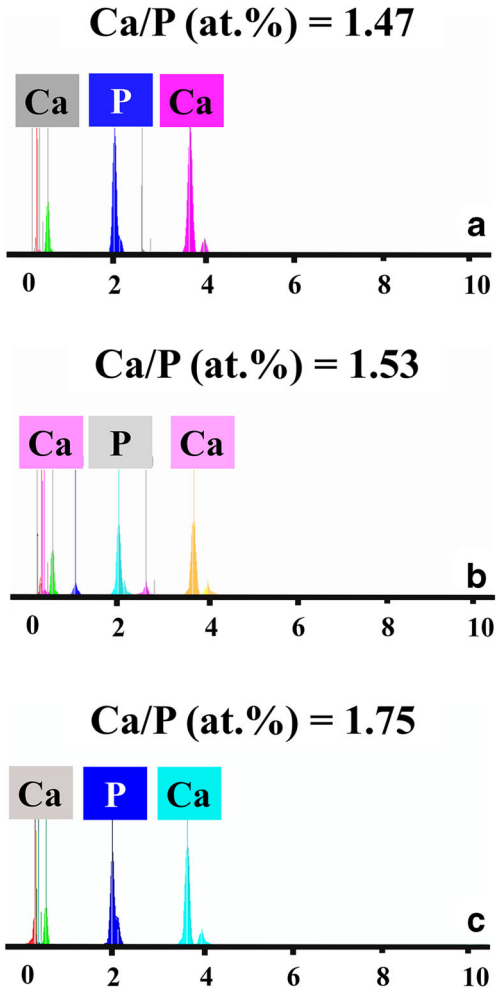

Fig. 7 EDX analysis of CP1G scaffolds after soaking in the SBF solution for **a** 3, **b** 7, and **c** 14 days

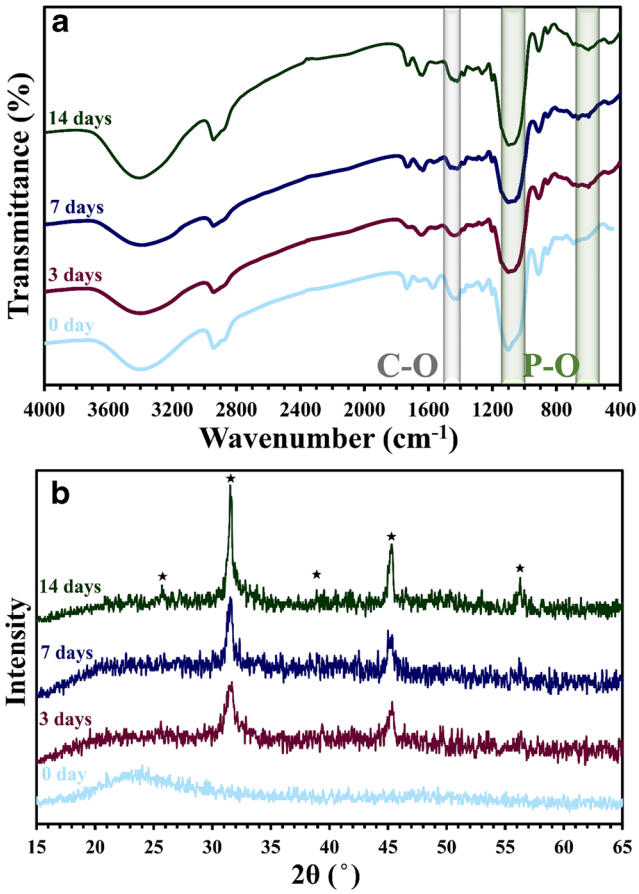

Fig. 8 **a** FTIR spectra and **b** X-ray diffraction pattern of CP1G scaffolds after different immersion time in the SBF solution

collagen stabilizing, cell attachment, bone extracellular matrix deposition, and induce osteoblastic differentiation, the effect of Si ion on the postpone of cellular proliferation is noticeable [13]. The amount of Si release is a critical factor and a high concentration of Si ions leads to cell apoptosis [52]. In this study, the low amount of cell proliferation on CP1G sample is related to Si ion release, but the moderate Si ion release on the following days accelerates cell proliferation in comparison to the control group.

The results of the ALP activity of cultured-MG-63 cells on the CP1G scaffold and the control group are presented in Fig. 9(c). The ALP activity reached 150 (U/L) after 3 days, followed by a slight increase on day 5. Enhancement in ALP activity illustrates the fact that an osteogenic function on the scaffolds can be carried out by cells. According to observation, the higher ALP activity of CP1G scaffolds in comparison to the control group showed a more exceptional ability to support cell differentiation after an incubation time of 3 and 5 days. These observations are compatible with the results of the MTT assay and cell culture, which reveal suitable biocompatibility properties of CP1G scaffolds for cell viability and proliferation.

4 Conclusion

Chitosan-PVA/GPTMS scaffolds with a different weight ratio of GPTMS were prepared by the freeze-drying method. In this investigation, the effect of cross-linker content on the performance of fabricated structures was studied. Based on SEM images, interconnected pores in scaffolds were illustrated in which the diameter of pores increased as a function of GPTMS content. The FTIR results showed that the blends of chitosan and PVA were cross-linked through the amine group of chitosan and C-OH of PVA with the epoxide ring of GPTMS. Increasing GPTMS content promoted the compressive strength of the samples. The degradation study indicated that enhancing the GPTMS content causes a decrease in water absorption as well as the degradation of scaffolds network. Immersion of the constructs in the SBF solution resulted in the formation of needle-like particles on the surface of samples, revealing the excellent bioactivity of the scaffolds. The MG-63 cells-scaffolds interactions indicated a desired

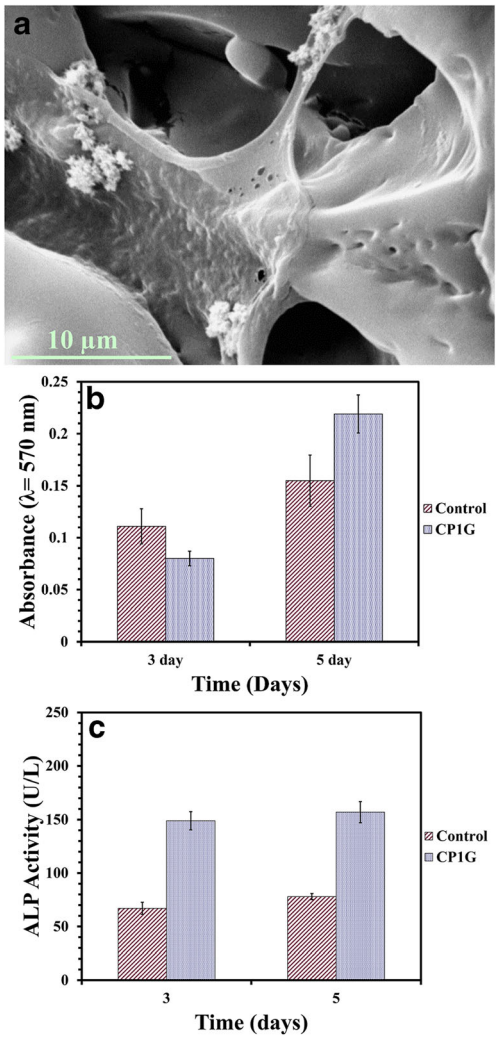

Fig. 9 **a** Attachment of MG-63 osteosarcoma cells seeded on scaffolds after 48 h, **b** The viability of MG-63 osteosarcoma cells on the surface of the scaffolds at day 3 and 5 after seeding was assessed using the MTT assay (O.D. value 570 nm), **c** Alkaline phosphatase (ALP) activity of MG-63 cells on CP1M scaffolds. (There were no statistically significant differences between test groups)

spreading of cells after 48 h. MTT assay showed that the portion of viable cells seeded onto the CP1G scaffold was much more than those seeded onto the control sample. This observation confirmed the biocompatibility of CP1G scaffolds with MG-63 cells. Finally, ALP activity results demonstrated that CP1G scaffolds might be a good choice for bone tissue engineering applications and further in-vivo studies.

References

1. Aldemir Dikici B, Dikici S, Karaman O, Oflaz H (2017) The effect of zinc oxide doping on mechanical and biological properties of 3D printed calcium sulfate based scaffolds. Biocybern Biomed Eng 37: 733–741. https://doi.org/10.1016/j.bbe.2017.08.007
2. Bandyopadhyay A, Dewangan VK, Vajanthri KY, Poddar S, Mahto SK (2018) Easy and affordable method for rapid prototyping of tissue models in vitro using three-dimensional bioprinting. Biocybern Biomed Eng 38:158–169. https://doi.org/10.1016/j.bbe.2017.12.001
3. Mohammadi Y, Soleimani M, Fallahi-Sichani M, Gazme A, Haddadi-Asl V, Arefian E et al (2007) Nanofibrous poly(epsilon-caprolactone)/poly(vinyl alcohol)/chitosan hybrid scaffolds for bone tissue engineering using mesenchymal stem cells. Int J Artif Organs 30:181–277
4. Kadir MFZ, Aspanut Z, Majid SR, Arof AK (2011) FTIR studies of plasticized poly(vinyl alcohol)–chitosan blend doped with NH4NO3 polymer electrolyte membrane. Spectrochim Acta Part A Mol Biomol Spectrosc 78:1068–1074. https://doi.org/10.1016/j.saa.2010.12.051
5. Ghorbani F, Zamanian A, Nojehdehian H (2017) Effects of pore orientation on in-vitro properties of retinoic acid-loaded PLGA/gelatin scaffolds for artificial peripheral nerve application. Mater Sci Eng C 77:159–172. https://doi.org/10.1016/j.msec.2017.03.175
6. Gutiérrez TJ, Alvarez VA (2017) Properties of native and oxidized corn starch/polystyrene blends under conditions of reactive extrusion using zinc octanoate as a catalyst. React Funct Polym 112:33–44. https://doi.org/10.1016/j.reactfunctpolym.2017.01.002
7. Haque MM-U, Puglia D, Fortunati E, Pracella M (2017) Effect of reactive functionalization on properties and degradability of poly(lactic acid)/poly(vinyl acetate) nanocomposites with cellulose nanocrystals. React Funct Polym 110:1–9. https://doi.org/10.1016/j.reactfunctpolym.2016.11.003
8. Li N, Liu F, Lu Q, Shi Y, Xiao C, Cheng B (2016) The preparation and study of poly(vinylidene fluoride)/ultrahigh-molecular-weight polyethylene/SiO2 hollow fiber membrane with network enhanced structure. React Funct Polym 109:64–69. https://doi.org/10.1016/j.reactfunctpolym.2016.10.005
9. Croisier F, Jérôme C (2013) Chitosan-based biomaterials for tissue engineering. Eur Polym J 49:780–792. https://doi.org/10.1016/j.eurpolymj.2012.12.009
10. Khor E, Lim LY (2003) Implantable applications of chitin and chitosan. Biomaterials 24:2339–2349. https://doi.org/10.1016/S0142-9612(03)00026-7
11. Gaaz T, Sulong A, Akhtar M, Kadhum A, Mohamad A, Al-Amiery A (2015) Properties and applications of polyvinyl alcohol, halloysite nanotubes and their nanocomposites. Molecules 20: 22833–22847. https://doi.org/10.3390/molecules201219884
12. Witt MA, Barra GMO, Bertolino JR, Pires ATN (2010) Crosslinked chitosan/poly (vinyl alcohol) blends with proton conductivity characteristic. J Braz Chem Soc 21:1692–1698. https://doi.org/10.1590/S0103-50532010000900014
13. Ghorbani F, Zamanian A, Behnamghader A, Daliri JM (2018) A novel pathway for in situ synthesis of modified gelatin microspheres by silane coupling agents as a bioactive platform. J Appl Polym Sci 46739. https://doi.org/10.1002/app.46739
14. Tonda-Turo C, Gentile P, Saracino S, Chiono V, Nandagiri VK, Muzio G et al (2011) Comparative analysis of gelatin scaffolds crosslinked by genipin and silane coupling agent. Int J Biol Macromol 49:700–706. https://doi.org/10.1016/j.ijbiomac.2011.07.002
15. Chen Q, Roether JA, Boccaccini AR (2008) Tissue engineering scaffolds from bioactive glass and composite materials. Top Tissue Eng 4:1–27
16. He X, Xu H, Li H (2015) Cr(VI) removal from aqueous solution by chitosan/carboxylmethyl cellulose/silica hybrid membrane. World J Eng Technol 03:234–240. https://doi.org/10.4236/wjet.2015.33C034
17. Fiamingo A, Campana-Filho SP (2016) Structure, morphology and properties of genipin-crosslinked carboxymethylchitosan porous

membranes. Carbohydr Polym 143:155–163. https://doi.org/10.1016/j.carbpol.2016.02.016
18. Jones JR (2015) Reprint of: review of bioactive glass: from Hench to hybrids. Acta Biomater 23:S53–S82. https://doi.org/10.1016/j.actbio.2015.07.019
19. Marcacci M, Kon E, Moukhachev V, Lavroukov A, Kutepov S, Quarto R, Mastrogiacomo M, Cancedda R (2007) Stem cells associated with macroporous bioceramics for long bone repair: 6- to 7-year outcome of a pilot clinical study. Tissue Eng 13:947–955. https://doi.org/10.1089/ten.2006.0271
20. Hench LL Third-generation biomedical materials. Science (80-) 2002(295):1014–1017. https://doi.org/10.1126/science.1067404
21. Sousa RA (2003) Coupling of HDPE/hydroxyapatite composites by silane-based methodologies. J Mater Sci Mater Med 14:475–487. https://doi.org/10.1023/A:1023471011749
22. Gomes M, Reis R, Cunha A, Blitterswijk C, de Bruijn J (2001) Cytocompatibility and response of osteoblastic-like cells to starch-based polymers: effect of several additives and processing conditions. Biomaterials 22:1911–1917. https://doi.org/10.1016/S0142-9612(00)00377-X
23. Ghorbani F, Zamanian A, Behnamghader A, Joupari MD (2018) Microwave-induced rapid formation of biomimetic hydroxyapatite coating on gelatin-siloxane hybrid microspheres in 10X-SBF solution. E-Polymers. https://doi.org/10.1515/epoly-2017-0196
24. Ren L, Tsuru K, Hayakawa S, Osaka A (2002) Novel approach to fabricate porous gelatin–siloxane hybrids for bone tissue engineering. Biomaterials 23:4765–4773. https://doi.org/10.1016/S0142-9612(02)00226-0
25. Arabi N, Zamanian A, Rashvand SN, Ghorbani F (2018) The tunable porous structure of gelatin-bioglass nanocomposite scaffolds for bone tissue engineering applications: physicochemical, mechanical, and in-vitro properties. Macromol Mater Eng 303:1700539. https://doi.org/10.1002/mame.201700539
26. Ghorbani F, Zamanian A (2018) Oxygen-plasma treatment-induced surface engineering of biomimetic polyurethane nanofibrous scaffolds for gelatin-heparin immobilization. E-Polymers 18:275–285. https://doi.org/10.1515/epoly-2017-0185
27. Kokubo T, Takadama H (2006) How useful is SBF in predicting in vivo bone bioactivity? Biomaterials 27:2907–2915. https://doi.org/10.1016/j.biomaterials.2006.01.017
28. Aidun A, Zamanian A, Ghorbani F (2019) Novel bioactive porous starch-siloxane matrix for bone regeneration: physicochemical, mechanical, and invitro properties. Biotechnol Appl Biochem 2018:1–29. https://doi.org/10.1002/bab.1694
29. Lowry OH, Rosebrough NJ, Farr AL, Randall RJ (1951) Protein measurement with the Folin phenol reagent. J Biol Chem 193:265–275
30. Wang D, Liu W, Feng Q, Dong C, Liu Q, Duan L, Huang J, Zhu W, Li Z, Xiong J, Liang Y, Chen J, Sun R, Bian L, Wang D (2017) Effect of inorganic/organic ratio and chemical coupling on the performance of porous silica/chitosan hybrid scaffolds. Mater Sci Eng C 70:969–975. https://doi.org/10.1016/j.msec.2016.04.010
31. Asadi-Eydivand M, Solati-Hashjin M, Farzad A, Abu Osman NA (2016) Effect of technical parameters on porous structure and strength of 3D printed calcium sulfate prototypes. Robot Comput Integr Manuf 37:57–67. https://doi.org/10.1016/j.rcim.2015.06.005
32. Rahman SM, Mahoney C, Sankar J, Marra KG, Bhattarai N (2016) Synthesis and characterization of magnesium gluconate contained poly(lactic-co-glycolic acid)/chitosan microspheres. Mater Sci Eng B 203:59–66. https://doi.org/10.1016/j.mseb.2015.10.011
33. Hsiao M-H, Tung T-H, Hsiao C-S, Liu D-M (2012) Nano-hybrid carboxymethyl-hexanoyl chitosan modified with (3-aminopropyl)triethoxysilane for camptothecin delivery. Carbohydr Polym 89:632–639. https://doi.org/10.1016/j.carbpol.2012.03.066
34. Guo R, Hu C, Pan F, Wu H, Jiang Z (2006) PVA–GPTMS/TEOS hybrid pervaporation membrane for dehydration of ethylene glycol aqueous solution. J Memb Sci 281:454–462. https://doi.org/10.1016/j.memsci.2006.04.015
35. Innocenzi P (2003) Infrared spectroscopy of sol–gel derived silica-based films: a spectra-microstructure overview. J Non-Cryst Solids 316:309–319. https://doi.org/10.1016/S0022-3093(02)01637-X
36. Shirosaki Y, Okayama T, Tsuru K, Hayakawa S, Osaka A (2013) In vitro bioactivity and MG63 cytocompatibility of chitosan-silicate hybrids. Int J Mater Chem 3:1–7
37. Enescu D, Hamciuc V, Ardeleanu R, Cristea M, Ioanid A, Harabagiu V et al (2009) Polydimethylsiloxane modified chitosan. Part III: preparation and characterization of hybrid membranes. Carbohydr Polym 76:268–278. https://doi.org/10.1016/j.carbpol.2008.10.026
38. Connell LS, Romer F, Suárez M, Valliant EM, Zhang Z, Lee PD et al (2014) Chemical characterisation and fabrication of chitosan-silica hybrid scaffolds with 3-glycidoxypropyl trimethoxysilane. J Mater Chem B 2:668–680. https://doi.org/10.1039/c3tb21507e
39. Chiono V, Tonda-Turo C (2015) Trends in the design of nerve guidance channels in peripheral nerve tissue engineering. Prog Neurobiol 131:87–104. https://doi.org/10.1016/j.pneurobio.2015.06.001
40. Shirosaki Y, Okayama T, Tsuru K, Hayakawa S, Osaka A (2008) Synthesis and cytocompatibility of porous chitosan-silicate hybrids for tissue engineering scaffold application. Chem Eng J 137:122–128. https://doi.org/10.1016/j.cej.2007.10.012
41. Ashammakhi N, Ndreu A, Yang Y, Ylikauppila H, Nikkola L (2012) Nanofiber-based scaffolds for tissue engineering. Eur J Plast Surg 35:135–149. https://doi.org/10.1007/s00238-008-0217-3
42. Gao C, Ito S, Obata A, Mizuno T, Jones JR, Kasuga T (2016) Fabrication and in vitro characterization of electrospun poly (γ-glutamic acid)-silica hybrid scaffolds for bone regeneration. Polymer (Guildf) 91:106–117. https://doi.org/10.1016/j.polymer.2016.03.056
43. Binsu VV, Nagarale RK, Shahi VK (2005) Phosphonic acid functionalized aminopropyl triethoxysilane-PVA composite material: organic-inorganic hybrid proton-exchange membranes in aqueous media. J Mater Chem 15:4823–4831. https://doi.org/10.1039/b511274e
44. Duan B, Yuan X, Zhu Y, Zhang Y, Li X, Zhang Y et al (2006) A nanofibrous composite membrane of PLGA-chitosan/PVA prepared by electrospinning. Eur Polym J 42:2013–2022. https://doi.org/10.1016/j.eurpolymj.2006.04.021
45. Vishal Gupta N, Shivakumar HG (2012) Investigation of swelling behavior and mechanical properties of a pH-sensitive superporous hydrogel composite. Iran J Pharm Res 11:481–493. https://doi.org/10.1021/la980982
46. Wang J, Fan X, Tian W, Wang Y, Li J (2011) Ring-opening polymerization of γ-glycidoxypropyltrimethoxysilane catalyzed by multi-metal cyanide catalyst. J Polym Res 18:2133–2139. https://doi.org/10.1007/s10965-011-9623-5
47. Yoon B-H, Kim H-E, Kim H-W (2008) Bioactive microspheres produced from gelatin–siloxane hybrids for bone regeneration. J Mater Sci Mater Med 19:2287–2292. https://doi.org/10.1007/s10856-007-3332-y
48. Li A, Shen H, Ren H, Wang C, Wu D, Martin RA et al (2015) Bioactive organic/inorganic hybrids with improved mechanical performance. J Mater Chem B 3:1379–1390. https://doi.org/10.1039/C4TB01776E
49. Liu W, Wu X, Zhan H, Yan F (2012) Synthesis of bioactive poly(-ethylene glycol)/SiO2-CaO-P2O5 hybrids for bone regeneration. Mater Sci Eng C 32:707–711. https://doi.org/10.1016/j.msec.2012.01.012
50. Gao C, Gao Q, Li Y, Rahaman MN, Teramoto A, Abe K (2013) In vitro evaluation of electrospun gelatin-bioactive glass hybrid

scaffolds for bone regeneration. J Appl Polym Sci 127:2588–2599. https://doi.org/10.1002/app.37946

51. Ghorbani F, Zamanian A, Behnamghader A, Joupari MD (2019) A facile method to synthesize mussel-inspired polydopamine nanospheres as an active template for in situ formation of biomimetic hydroxyapatite. Mater Sci Eng C 94:729–739. https://doi.org/10.1016/j.msec.2018.10.010

52. Shie MY, Ding SJ, Chang HC (2011) The role of silicon in osteoblast-like cell proliferation and apoptosis. Acta Biomater 7:2604–2614. https://doi.org/10.1016/j.actbio.2011.02.023